Journal of Power Sources 239 (2013) 294–307

Contents lists available at SciVerse ScienceDirect

Journal of Power Sources

journal homepage: www.elsevier.com/locate/jpowsour

Battery state of the charge estimation using Kalman filtering

M. Mastali [a], J. Vazquez-Arenas [b], R. Fraser [a], M. Fowler [c,*], S. Afshar [a], M. Stevens [d]

[a] Mechanical and Mechatronic Engineering Department, University of Waterloo, 200 University Avenue West, Waterloo, ON N2L 3G, Canada
[b] Universidad Autonoma Metropolitana-Iztapalapa, Departamento de Qumica, Av. San Rafael Atlixco 186, Mexico D.F. 09340, Mexico
[c] Chemical Engineering Department, University of Waterloo, 200 University Avenue West, Waterloo, ON N2L 3G1, Canada
[d] CrossChasm Company, 2-60 Northland Road, Waterloo, ON N2V 2B8, Canada

HIGHLIGHTS

- We model the dynamical behavior of the Li-ion batteries.
- We use two types of Kalman filtering include extended and dual extended.
- Two different geometries (cylindrical and prismatic) for batteries are considered.
- The SOC of the batteries in a dynamical environment is accurately predicted.
- New physical insights are provided through analysis of the Kalman filter parameters.

ARTICLE INFO

Article history:
Received 20 January 2013
Received in revised form
20 March 2013
Accepted 22 March 2013
Available online 2 April 2013

Keywords:
Kalman filter
Battery SOC estimation
Hybrid electric vehicles
Plug-in hybrid electric vehicles

ABSTRACT

Battery management system (BMS) requires an accurate prediction the remaining energy level or state of charge (SOC) of the cell or battery pack. However, in electric vehicles, batteries experience a dynamic operational environment whereby the simple algorithms employed in the portable devices to predict SOC, such as coulomb counting, are insufficient for this purpose. To address this problem, a Kalman filtering method is used to estimate the state of the charge of two different commercial lithium-ion batteries, with new physical insight being provided through an analysis of the Kalman filter covariance noise parameters. For example, the effect of geometry of the battery on value of these parameters is discussed. Different models are developed, tested and incorporated in the filter design. Subsequently, two types of Kalman filters including the extended Kalman filter and dual extended Kalman filter are implemented in order to predict the state of charge of the batteries. It is shown that the Kalman filtering can predict state of the charge of the battery with maximum 4% error.

1. Introduction

The drive toward higher fuel efficiency, lower emission and energy security is driving the rapid advancement of hybrid and electric vehicle technologies, and both of these vehicle technologies require an energy storage system. Lithium-ion (Li-ion) batteries have become popular as energy storage devices because they have very high energy densities, are a low maintenance battery, there is no memory effect, and there is low self-discharge compared to nickel-cadmium technologies. Despite its overall advantages, lithium-ion technology requires power electronic (i.e. a battery management system (BMS)) for cell voltage balancing within a pack of cells, a protection circuit to prevent overcharging which is a safety concern. Over-discharge of the cells will lead to degradation and cell failure. Thermal extremes limit performance and cause cell degradation.

Thus, technical difficulties in the design process of the vehicles have limited its performance under dynamic operating conditions experienced in vehicle operation. One of the most important battery control and monitoring parameters is the estimation of the state of charge (SOC) of the battery, since it determines the amount of energy available and thus the range of the vehicle under all electrical or electrical assist operation. Most importantly, the life of the battery if operated within a certain range of SOC can reduce degradation and thus reduce the life cycle costs. Therefore, correct estimation of the SOC of the battery has become crucial in the manufacture of Battery Electric (BEV), Plug-in Hybrid Electric (PHEV), and Hybrid Electric Vehicles (HEV). These vehicles experience a dynamic power demand profile, with peaks in power draw as well as a wide range of SOC change [1].

* Corresponding author. Tel.: +1 519 888 4567x33415; fax: +1 519 746 4979.
E-mail address: mfowler@uwaterloo.ca (M. Fowler).

0378-7753/$ – see front matter © 2013 Elsevier B.V. All rights reserved.
http://dx.doi.org/10.1016/j.jpowsour.2013.03.131

Methods to estimate SOC in small electronic devices have been implemented for several years [2]. However, different requirements are demanded by the batteries in the vehicles, whereby relying on these methods may be totally inaccurate for vehicle purposes. Plett [3] compared battery applications for portable electronic devices and EVs against those utilized in HEVs, concluding that the latter one is much more demanding than the other two applications in terms of battery usage. The parameters used for this comparative study were the maximum rate of the charge and discharge, duty cycle, accuracy needed to estimate the SOC, and lifetime of the battery. It was concluded that for all the aforementioned parameters, the HEV environment involves more challenges when the battery management systems (BMS) are engaged. Particularly, SOC estimation within the accuracy range demanded for the HEVs presents a serious challenge for the BMSs.

For this reason, the objective of this work is to solve the described problem by developing a robust Kalman filter method to estimate the SOC of commercial batteries implemented in HEV and PHEV. In addition, we provide a more complete description for implementing the Kalman filter in order to make it more accessible to a greater number of battery researchers. By comparing the noise parameters used in Kalman filtering of two cylindrical and prismatic $LiFePO_4$ batteries, some physical descriptions are also provided to explain the reason behind the difference between the values of these parameters.

1.1. Background

Some research has been carried out to develop methods capable to estimate the SOC of the batteries for vehicle applications [4–13]. In the most recent published work Andre et al. have fitted a Kalman filter and support vector machine (SVM) algorithm to NMC cathode cells. Piller et al. have published an extensive review of different methods applied to determine the SOC [14]. To this concern, the most frequent methods for SOC estimation utilized are summarized below, and include:

1. coulomb counting,
2. open circuit voltage (OCV) estimation,
3. electrochemical impedance spectroscopy (EIS), and
4. filtering.

Among these, coulomb counting is the most common used for small electronic devices. This method employs a very simple and intuitive principle entailing that the number of electrons transferred to the battery during the charge period are equal to the number of electrons transferred from the battery during the discharge period. This can be formulated as

$$\mathrm{SOC} = \mathrm{SOC}_0 + \frac{1}{C_\mathrm{n}} \int (I_\mathrm{batt} - I_\mathrm{loss})\mathrm{d}t \quad (1)$$

where SOC_0 is initial SOC, C_n is the nominal capacity of the battery in As, I_batt is the discharging (positive) or charging (negative) current of the battery in A, and I_loss is the current consumed by the loss reactions in A.

However, the coulomb counting method presents two main problems. First, the charging current supplied by an external power source is not totally used, and thus calculations of the I_loss are required. This calculation is not straightforward, and it may introduce a considerable error in the lack of a precise determination [14]. Second, an accurate measurement of the current is crucial in this technique, whereby more expensive sensors are required. In general, two different types of sensors are used: Hall Effect and current shunt sensors. A Hall Effect sensor measures the magnetic field around a wire and then estimates the current through it by using Ampere's law. On the other hand, the current shunt sensor is a very small resistance used in series with the circuit to measure the voltage drop. Ohm's law is subsequently used to calculate the current flow in the wire. Although the current shunt sensors provide more precise current measurements, the Hall Effect sensors are easier to install. However, none of them can provide accurately measurements for SOC estimation via coulomb counting. Therefore, a better method needs to be applied for these purposes. In portable devices recalibration of the SOC estimation often requires complete discharge of the battery which has degradation impacts on cells, as well as being impractical in vehicle applications.

The OCV estimation is a method regularly used for SOC prediction. It relies on the fact that under open circuit conditions (i.e. current equals zero), the measured voltage can be related to the battery SOC using the OCV diagram. Fig. 1 shows the OCV diagram of a battery fabricated with $LiFePO_4$ cathodes. However, the use of this method leads to some problems in SOC estimation. The OCV–SOC relation highly depends on the chemistry, temperature, and State of the Health (SOH) of the battery. As battery ages, the OCV diagram changes slightly, whence its use for SOC estimation turns out to be inaccurate. In Li-ion technology the discharge performance is 'flat' with limited change in voltage over a wide range of SOC making estimation of SOC difficulty. The prediction of this dynamic change is especially difficult as a result of the complex duty profile and environment within the HEV and PHEV. In addition, the OCV is also affected by temperature, and a single OCV diagram cannot be utilized to account for different temperatures. It is worth to highlight from Fig. 1 that for the SOC range between 10 and 90%, wherein the HEV and PHEV mostly operate, the OCV changes approximately by 0.2 V. Consequently, a small inaccuracy in the voltage measurement yields a large error in SOC estimations. From an implementation standpoint, an equivalent circuit model can be used to model the terminal voltage of the battery at OCV which will allow for the electrical connections within a pack of cell. This type of model will be discussed in Section 3.

The third technique studied in this work is the Electrochemical Impedance Spectroscopy (EIS). Considerable research has been devoted in this area in order to estimate SOC and SOH. Further details of the SOC measurement in batteries through EIS can be consulted in Ref. [16]. The basis of this technique is to consider that the resistance of the electrochemical reaction is due to different phenomena that can be separated including the electrical impedance and mass transfer resistance. Electrochemical Impedance Spectroscopy (EIS) is applied for the characterization of electrode

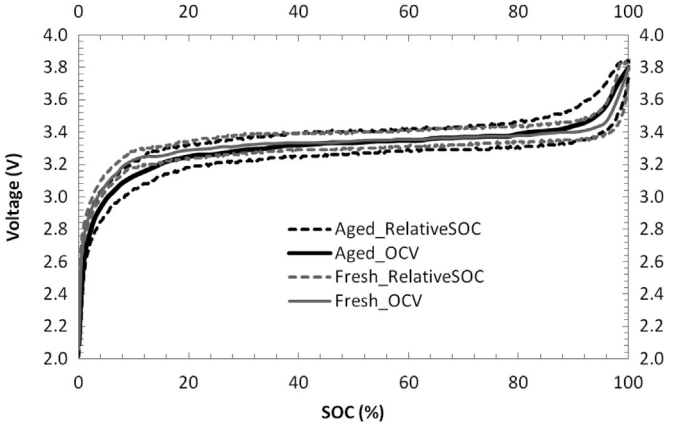

Fig. 1. Open-circuit voltage for fresh and aged batteries as a function of state-of-charge [15].

processes and complex interfaces, through the measurement of the system response to the application of a periodic small amplitude ac signal. This allows for examination of various electrode processes such as the ionic transfer and electrons transfer. Of interest to this study is that when the SOC decreases, the contribution of the resistance associated with diffusion phenomena becomes higher, and the Nyquist plot exhibits a 45° linear-slope. Fig. 2 exhibits the Nyquist plot of a Li-ion battery for different SOCs. In spite of the large number of papers published on this subject [16–19], this method is rarely used as the SOC estimator. This stems from the fact that the instrumentation is complex and expensive. Moreover, the measurement is highly affected by the localized electrode temperature and aging of the electrode materials. Hence, this method is typically used for quality control and to a limited extent to provide information about the SOH in academic studies rather than a practical measure of SOC. Please refer to [20], for further information concerning impedance measurements for Li-ion batteries.

Recently, adaptive methods including fuzzy logic, neural networks, adaptive observers, and Kalman filters are widely used to estimate SOC [21]. Among these techniques, the Kalman filtering seems to be very promising [4–13]. In practice, it filters the input signals and output signals of the system to accurately predict the dynamic state of the system. Since the equations of this filter involve basic matrix operations, it can be easily implemented on a Digital-Signal-Processing (DSP) chips, making it valuable from a practical point of view. One of the advantages of Kalman filtering is that provides the error bound for each estimated state [3]. In addition, this method can be utilized for parameter estimation, whereby the system identification and state estimation can be implemented at the same time.

Although Kalman filtering has lately received considerable attention [4–13], some gaps are still observed in this area. To this concern, the effect of battery type on the parameters of the Kalman filter has not been assessed yet, whereby only one battery chemistry and geometry are typically analyzed in each study. In this work, two different geometries of Li-ion batteries (cylindrical and prismatic) are considered, and by comparing the covariance noise parameters of the Kalman filters, some physical insights are discussed considering the magnitude of these values. Moreover, a good comparison over the different equivalent circuits of the battery and their impact on the accuracy of the Kalman filtering is provided. Both methods, extended and dual extended Kalman filters are described in detail, in order to expedite their implementation for practical applications in HEV or PHEV. The next section describes the experiments conducted using two different batteries, whereas section three provides details of the development and implementation of different models considered to account for the behavior of the batteries. In the last section, these models are utilized to estimate SOC of the battery, and the most suitable Kalman filtering is selected based on the performance of the filter to predict the SOC accurately.

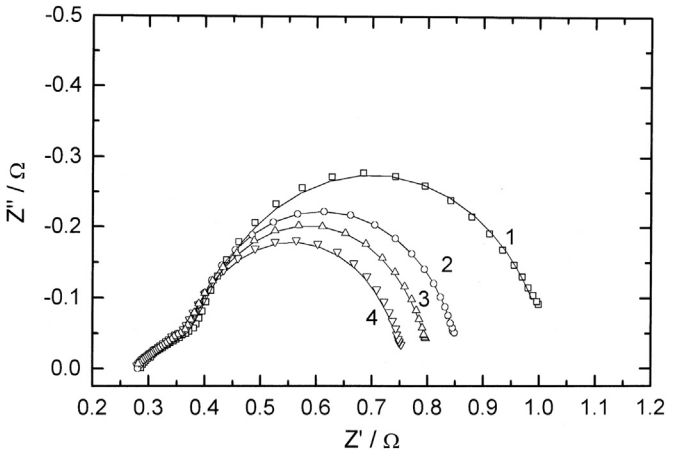

Fig. 2. Impedance spectra of lithium-ion battery at SOC ≃ 0 (1), 0.14 (2), 0.28 (3), 0.42 (4) [18].

2. Battery experiment

A comparison of the performance of different proposed methods utilized to estimate SOC is carried out through experimental data. To this concern, an experimental setup for testing batteries containing $LiFePO_4$ cathodes was designed to collect the data. This was developed in such a way that simulates driving conditions for real HEV and is also a scaled-down adaptation of a HEV powertrain. The experimental setup contains three major components: the battery, regenerative source (which simulates the regenerative braking of a real vehicle), and a load box (which simulates the motor). The schematic diagram of the test stand is depicted in Fig. 3.

The batteries tested in the facility, shown in Fig. 3, were A123 cylindrical 26650 Li-ion batteries [23]. These batteries are commonly used in HEV, contain cathodes of $LiFePO_4$ and present a nominal voltage of 3.8 V. Moreover, they can provide a maximum continuous current of 60 A, or up to 120 A for peak currents during 10 s. The load box mounted on the test stand is a TDI Dynaload RBL232 50-150-800. This part was added to the test stand to resemble the behavior of an electric motor which initiates the load on the batteries. A Lambda ZUP 20-40-800 model AC/DC power source was integrated with the setup to charge the cells. The Lambda ZUP 20-40-800 model was selected based on its compatibility with the recharge requirements for the A123 Li-ion batteries. This setup was also equipped with a controller which is able to read the desired drive cycles and then drive the experimental setup according to the drive cycle's power demand data. Further details about this test setup can be found in Ref. [22].

In order to mimic the environment of the batteries in a HEV, the batteries were dynamically subjected to a series of charge and discharge cycles. Fig. 4 shows the current profile, whose duration was longer than 45,000 s. Positive current represents discharge from the battery and negative current is charging the cells. For better appreciation, the charging periods of the last cycles are expanded in the inset shown on the right part of the figure. The cycling of the batteries is started with a pre-test run at very slow charge and discharge rates, to position the battery at the same initial SOC. Then, the battery went through a series of high rate charge and discharges. The discharge process is designed to occur at maximum discharge current of 60 A. During this time, the cell was partially discharged (almost to 55% SOC). After 20,000 s, the depth of discharge (DOD) was gradually lowered for each discharge period such that at the end of the test the DOD of the last discharge period was around 5%. Furthermore, the charging process was

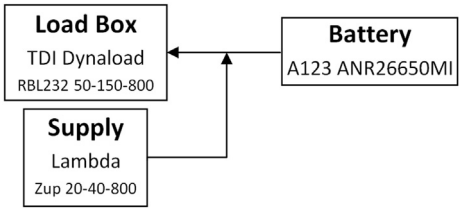

Fig. 3. Battery testing apparatus [22].

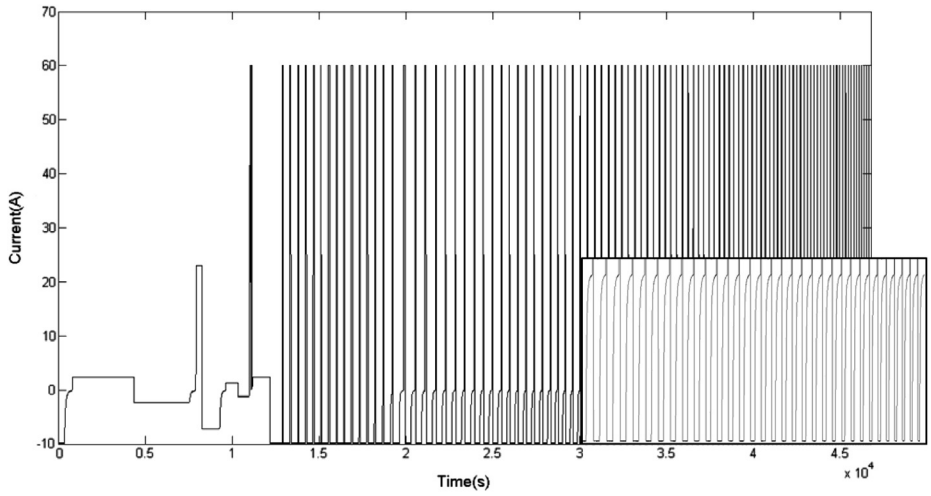

Fig. 4. Current profile of the battery during the dynamic test which resembles the HEVs environment.

comprised of two regions: the first part was a constant charging current (10 A) followed by a period of a constant voltage (3.8 V) until the current reached zero. This type of charge profile commencing around 19,000 s was chosen to ensure that the battery reached the 100% SOC at the end of each charging process. The experimental data were used to identify the parameters of the battery model described in Section 3, and to predict the SOC described in Section 4. In the next section, the models utilized to account dynamically for the behavior of the batteries are developed.

3. Model development

Two sets of equations are required to estimate SOC using a Kalman filtering signal processing technique, as discussed in Section 4. The first set is called the 'process model' where a discrete form of the coulomb counting equation (Eq. (1)) is commonly used. The second set is called 'measurement model' and is utilized to correct the error of the process model estimation, and to reduce the uncertainty. This model should provide a correct relation between the states, inputs and outputs of the system. In this paper, the state of the system is SOC, the input of the system is measured current, i, and the output is terminal voltage, V. The measurement model has the form of $V_k = f(\mathrm{SOC}_k, i_k, \theta_k)$; where θ is the parameters of the model and subscript k shows the kth time step. This section describes the measurement models, and is intended to find an appropriate measurement model for being used in the Kalman filtering process, as well as its parameters. Parameters for the measurement models can be classified in two categories: fixed and varying parameters. They are explained in detail in the following paragraphs. It is worth to mention that there is another approach to account for the behavior of a Li-ion battery through modeling. In this approach, physics based models such as the single particle (SP) model or any other type of electrochemical reduced models are considered [24,25]. However, the use of this type of models is beyond the scope of this work and generally involves much more computational time and effort.

Both types of parameters use the OCV diagram of the battery to relate the SOC of the battery to its voltage under load. They add or subtract some terms such as voltage drop across the battery with the aim of equalizing the terminal voltage, e.g. current flow to OCV relation. Therefore, the first requirement of the model is to calculate the OCV of the battery as a function of SOC. The easiest way to obtain this relation is to charge and discharge the battery at very slow rates to the cell's voltage limits prescribed by the manufacturer. In practice, the OCV is the average of the charge and discharge curves. Fig. 5 shows the charge, OCV and discharge curves of A123 battery used for the tests. To obtain these curves, the battery was charged and discharged at 0.2C, and the OCV was calculated from the obtained curves.

3.1. Fixed-parameter model

Two types of models will be considered in this category: simple model, and zero-sate hysteresis model [26].

3.1.1. Simple model

In the simple model, the terminal voltage of the battery is estimated using a very simple model depicted in Fig. 6. This model can be formulated as

$$V_k = \mathrm{OCV}(\mathrm{SOC}_k) - Ri_k \tag{2}$$

It should be noted that the resistance in the Eq. (2) depends on whether the battery is being charged or discharged and different values of R for charging and discharging is replaced in it [26].

To identify the parameters of the simple model, the off-line identification using Least Squares Estimation (LSE) theory is employed since the parameters are constant, and the model is linear with respect to the parameters. Thus, the first step is to form the overvoltage vector and current matrix as described below:

$$Y = \begin{bmatrix} V_1 - \mathrm{OCV}(\mathrm{SOC}_1) \\ V_2 - \mathrm{OCV}(\mathrm{SOC}_2) \\ \vdots \\ V_n - \mathrm{OCV}(\mathrm{SOC}_n) \end{bmatrix}, H = \begin{bmatrix} i_1^+ & i_1^- \\ i_2^+ & i_2^- \\ \vdots & \vdots \\ i_n^+ & i_n^- \end{bmatrix}$$

where the i_k^+ equals i_k if $i_k > 0$, the battery is discharging, and i_k^- equals i_k if $i_k < 0$, the battery is charging, otherwise they are zero. By introducing Y and H into Eq. (2), it has the form $Y = H\widehat{R}$, where $\widehat{R} = [R^+, R^-]^T$ is the unknown vector of parameters. In this vector, R^+ and R^- denote internal resistance of the battery during discharge and charge periods, respectively. Using the known Y and H, the unknown vector can be calculated by LSE method as $\widehat{R} = (H^T H)^{-1} H^T Y$. The simple model is completely defined when the constant $\widehat{R}$ vector and the lookup table for OCV as a function of SOC are estimated and plugged in the Eq. (2).

Fig. 7 shows the result of the simple model, simulating the voltage profile for a single cycle. As observed, a good quality fit is

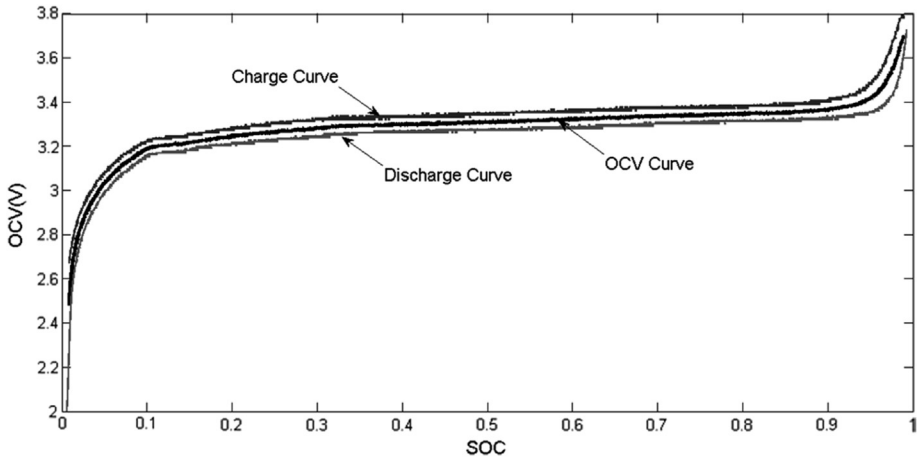

Fig. 5. Charge, OCV, and discharge curves of A123 battery.

obtained between the measured and predicted voltage, except for the region of constant voltage at the end of the cycle. This deviation is probably due to the hysteresis effect which is not incorporated in the simple model.

3.1.2. Zero-state hysteresis model

The hysteresis is a characteristic of a system where by changing the current course from charge to discharge, the output voltage of the cell does not trace back along the same voltage profile. This behavior of the system can be quantified by utilizing Fig. 5. The difference between the charging and discharging curves divided by two, all minus the effect of the voltage drop due internal resistance (Ri_k), and the result is taken as the hysteresis effect. The magnitude of the hysteresis is shown in Fig. 8 as a function of the SOC.

It can be seen from Fig. 8 that the hysteresis is almost constant in most of the SOCs and is less than 1% of the overall cell voltage. Therefore, it is reasonable to consider the hysteresis as a constant parameter in the measurement model and use the following form called zero-state hysteresis model.

$$V_k = \mathrm{OCV}(\mathrm{SOC}_k) - Ri_k - s_k M \tag{3}$$

where the parameter M is the hysteresis and s_k depends on the direction of the current and has adjustable memory during the rest period. The parameter s_k is defined as

$$s_k = \begin{cases} 1, & i_k > \varepsilon \\ -1, & i_k < -\varepsilon \\ s_{k-1}, & |i_k| \le \varepsilon \end{cases}$$

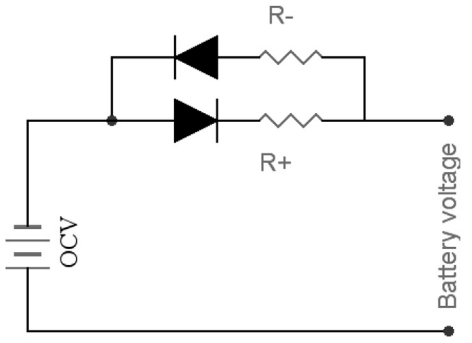

Fig. 6. Circuit of simple model, R^+ and R^- are charge and discharge resistances, respectively.

where the ε is a small positive constant number.

Similar to the simple model, LSE theory is used to identify the parameters since they are constant and the model is linear with respect to the parameters. The vector Y and matrix H are defined as

$$Y = \begin{bmatrix} V_1 & -\mathrm{OCV}(\mathrm{SOC}_1) \\ V_2 & -\mathrm{OCV}(\mathrm{SOC}_2) \\ \vdots & \vdots \\ V_n & -\mathrm{OCV}(\mathrm{SOC}_n) \end{bmatrix}, H = \begin{bmatrix} i_1^+ & i_1^- & s_1 \\ i_2^+ & i_2^- & s_2 \\ \vdots & \vdots & \vdots \\ i_n^+ & i_n^- & s_n \end{bmatrix}$$

and then the parameter vector ($\theta = [R^+, R^-, M]^T$) is obtained as described for the simple model. The result for a single cycle of this model is shown in Fig. 9. Evidently, this model predicts better the battery voltage during the last portion of the cycle than the simple model. However, the result shown in Fig. 9 is just for one cycle (e.g. first one). An appropriate model should regenerate the output of the battery for all current inputs, but this cannot be precisely addressed when constant parameters are used in the model. Thus, in order to tackle the dynamics of the system with different input currents, a model allowing the variation of the parameters needs to be developed.

3.2. Varying-parameter model

By using the zero-state model, the prediction of the battery voltage improves considerably, yet it is not adequate to simulate the behavior of the battery under dynamic environments like HEV and PHEV. In addition, the zero-state model cannot detect the slow variation of the hysteresis while changing the current direction. It just fluctuates between the positive and negative values of the identified hysteresis constant. Consequently, it is desired to add the hysteresis of the battery as another state of the system. Augmenting the hysteresis with the SOC in the state vector and estimating both OCV and SOC using a Kalman filtering approach addresses the discussed problems of the zero-state model. In this work, the hysteresis-state model proposed by Plett [26] is used according to the following formulation:

$$\frac{\mathrm{d}h(\mathrm{SOC}, t)}{\mathrm{dSOC}} = \gamma \mathrm{sgn}\left(\dot{\mathrm{SOC}}\right)\left(M\left(\mathrm{SOC}, \dot{\mathrm{SOC}}\right) - h(\mathrm{SOC}, t)\right) \tag{4}$$

where $M(\mathrm{SOC}, \dot{\mathrm{SOC}})$ is the maximum polarization due to battery hysteresis as function of SOC and its rate of change. Moreover, $M(\mathrm{SOC}, \dot{\mathrm{SOC}})$ has the positive value during charging and negative during discharging. Eq. (4) relates the rate of the hysteresis change to its distance from M. This form of equation results in an

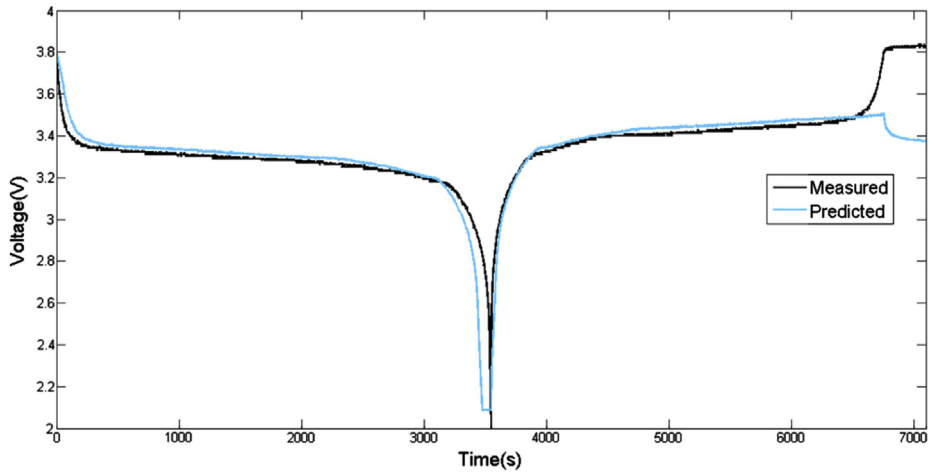

Fig. 7. Simple model voltage prediction for a single cycle.

exponential decay of hysteresis to the major loop. The term γ is a tuning factor and controls the rate of decay. Finally, the term sgn(SOC) has a stabilizing effect on the model. By using this type of hysteresis, the output of the model yields

$$V_k = \mathrm{OCV}(\mathrm{SOC}_k) - Ri_k + h_k \quad (5)$$

The simulation of the battery voltage by the hysteresis-state model is reported in Fig. 10 for one cycle. A comparison of Fig. 10 with Figs. 7 and 9 reveals that the hysteresis-state model presents a better prediction of the battery voltage over the simple and zero-state hysteresis models. Additionally, a very good quality can be observed over the entire range of voltage when this model is used. Fig. 11 compares the capability of the hysteresis-state and zero-state hysteresis model to predict the output voltage of the battery under a dynamic environment. As previously mentioned, constant parameters restrict the capabilities of the zero-state hysteresis model to accurately predict the output voltage. Despite this, the hysteresis-state model shows an acceptable performance regardless of the dynamics of the system.

4. SOC estimation

This section briefly describes the Kalman filtering method and its implementation to estimate the SOC of the battery. However, more details are provided which make it easier to follow the procedure and implement the explained Kalman filters. Two methods of Kalman filtering are considered: extended Kalman filter and dual extended Kalman filter. The results of these filters are also compared against the coulomb counting method. In the first part of this section the method is developed and applied to cylindrical cells, and then the developed methodology is applied to prismatic cell data.

In general, for a linear system, Kalman filtering provides an optimal estimate of the system states which are not directly measurable. However, in the case of nonlinear systems such as batteries, Kalman filtering is still an intelligent way to determine the states of the system. These states provide a comprehensive representation of the internal condition of the system and summarize contributions of all past inputs of the system. A Kalman filter computes the states of the system by utilizing a process model, a measurement model and a set of noisy measurements of inputs and output of the system. While the process model contains all information about the system dynamics, the measurement model relates the outputs of the system to its inputs and states. The process and measurement models predict the present state and correct the raw state estimation obtained from the process model [3,22], respectively. A complete description of the Kalman filtering process is reported in reference [27].

In the design procedure of the Kalman filters applied to the estimations of the battery states, the current of the battery is the

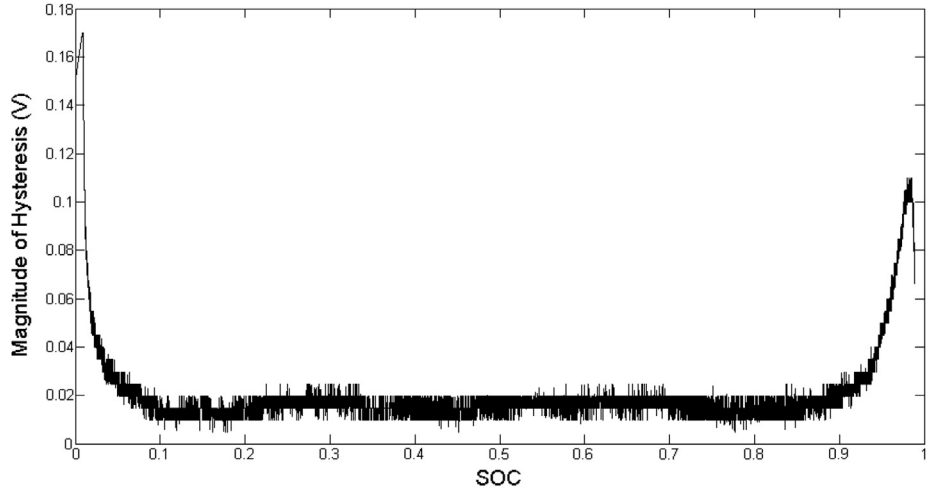

Fig. 8. Magnitude of the difference between charge and discharge OCV a function of SOC (i.e. magnitude of the hysteresis).

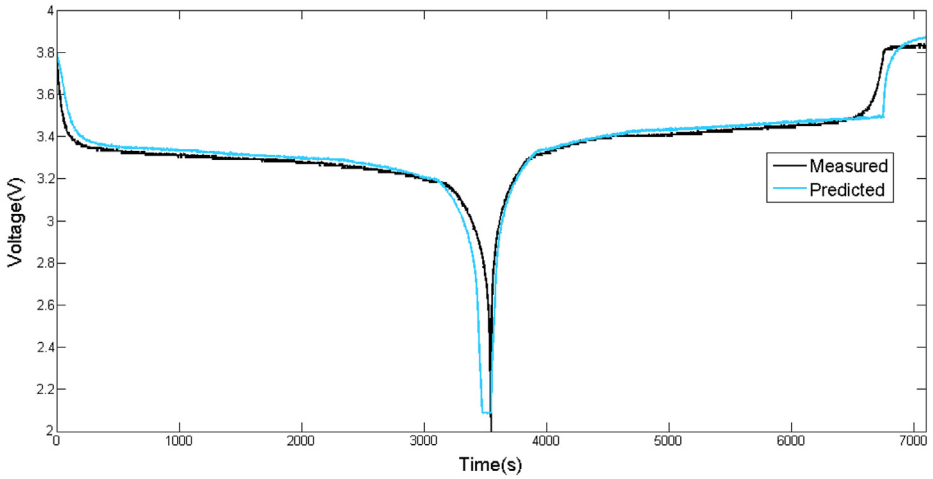

Fig. 9. Zero-state hysteresis model voltage prediction for a single cycle.

measured input, whereas the voltage measured on the battery terminals is the output. The states required to be estimated include state of charge, state of health, hysteresis, etc. In this work, the state considered is the SOC and the hysteresis will be incorporated in the state vector as well as the SOC when the hysteresis-state model is studied. The process model needs to relate the input current to the SOC, whereby the coulomb counting equation can be ideal for this purpose. Discretizing Eq. (1) in terms of time results in

$$\mathrm{SOC}_k = \mathrm{SOC}_{k-1} + \frac{\eta_i i_{k-1} \Delta t}{C_\mathrm{n}} \tag{6}$$

where η_i is the coulombic efficiency of the battery during charge and discharge. This factor is the ratio between consumed over available electrons in the charging or discharging processes. In other words, the energy provided by an external energy source cannot be totally stored in the battery due to mainly secondary reactions such as Li plating and electrolysis of water [22]. This ratio is assumed to be 0.992 during the charging period and 1.0 during discharging [22,26].

When the hysteresis-state model is considered for Kalman filtering, the hysteresis is also considered as a part of the state vector. Therefore, a different process model is incorporated in the Kalman filter design, connecting the hysteresis to the input current. The discrete version of the solution of Eq. (4) provides this relation:

$$h_{k+1} = \exp\left(-\left|\frac{\eta_i i_k \gamma \Delta t}{C_\mathrm{n}}\right|\right) h_k + \left(1 - \exp\left(-\left|\frac{\eta_i i_k \gamma \Delta t}{C_\mathrm{n}}\right|\right)\right) \times M\left(\mathrm{SOC}, \dot{\mathrm{SOC}}\right) \tag{7}$$

The measurement models map the input current and states of the battery to the output voltage. Details of these models were discussed in Section 3. From this point, only the zero-state hysteresis and hysteresis-state models are considered. Table 1 summarizes these models.

First, we apply the Kalman filter process on the zero-state hysteresis model. The process model has a linear structure whereas the measurement relation is not linear with respect to the SOC, whence a nonlinear version of Kalman filter should be utilized. For this model, the extended Kalman filter was chosen and implemented since the constant parameters of the system have been already estimated. Note that the focus of this paper is on the application and implementation of the Kalman filter to the battery SOC, whereby detailed algorithms of the Kalman filter itself should be consulted in Ref. [27]. The implementation of the extended Kalman filter using the zero-state battery model is summarized in Table 2.

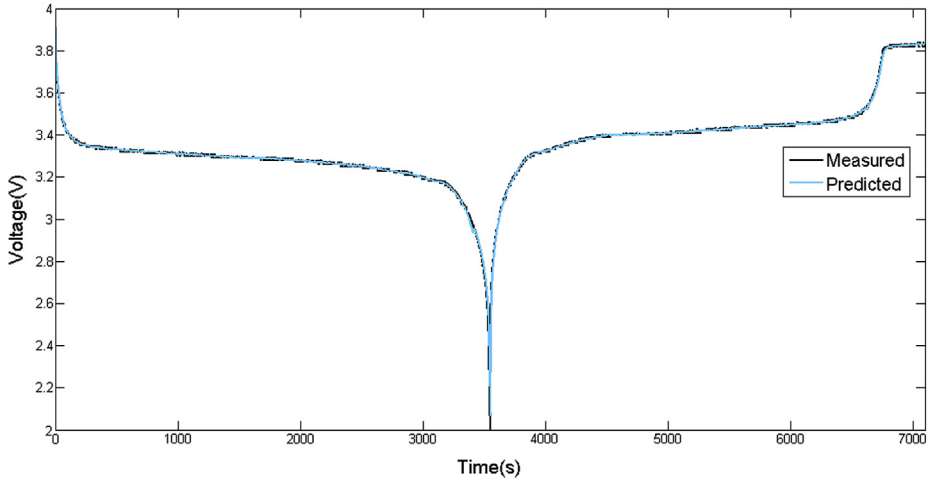

Fig. 10. Hysteresis-state model voltage prediction for a single cycle.

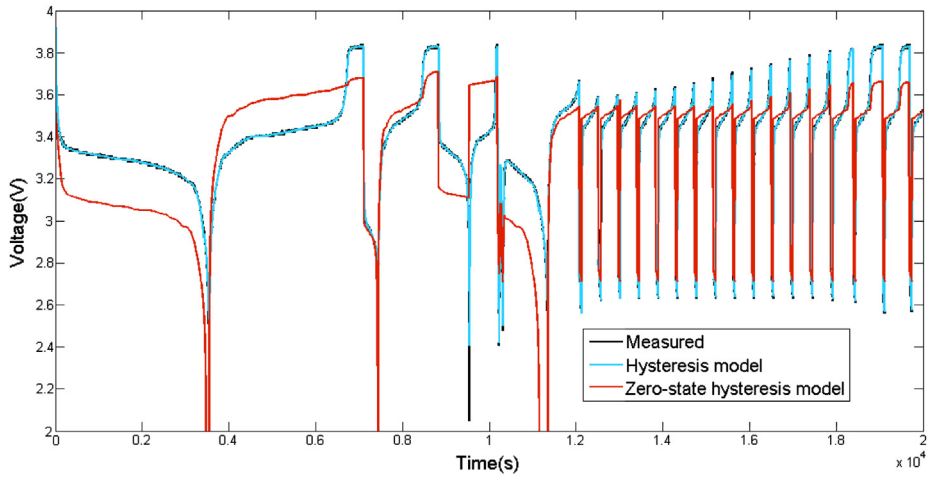

Fig. 11. Comparing the hysteresis-state and zero-state hysteresis model in a dynamic environment.

In order to calculate the $\hat{C}_k$, the OCV lookup table and a central difference method around the SOC_k^- is used.

$$\hat{C}_k = \frac{OCV(SOC_k^- + \delta) - OCV(SOC_k^- - \delta)}{2\delta} \quad (8)$$

The value of δ is arbitrarily a small number perturbation, which represents the change in SOC within the model and selected to be 0.001 in this study. The next step to implement the extended Kalman filter is to determine the variances introduced in the model. The process noise parameter practically covers the uncertainties which are ignored in the modeling procedure and the input measurement noise. In this study, it is assumed that the process noise is entirely derived from the inaccuracy in the current measurement. A simple calculation of the accuracy of the sensors leads to the current variance of $P_w = 1.3 \times 10^{-10}$ [22]. However, this value may be small compared to the capacity of the battery, causing a very small error. Similarly, the measurement error is determined from the variance of the voltage measurement for the sensors. This value is around $P_v = 1.8 \times 10^{-4}$ [22].

Fig. 12 depicts the results of coulomb counting method applied to the experimental data during the 45,000 s of cycling. In this figure, the experimental discharge line was obtained from the experimental data using a coulomb counting method starting from 19,000 s where the battery cell was fully charged at the end of each charging period. This observation was based on the current profiles obtained in Fig. 4 starting from this time. As it is detectable, this method poorly predicts the SOC of the battery. This is due to accumulative error problem in the coulomb counting method and the fact that coulomb counting does not have a correcting mechanism.

The result of SOC estimation utilizing the extended Kalman filter is shown in Fig. 13. This figure is divided into three regions. In the first region the battery goes through a series of slow rate charge and discharge cycles whereas in the second region it goes through a series of fast rate charge and discharge cycles. The measured voltages reported in Fig. 11 reveal that in the second time period, the battery does not get fully charged. In the third region, the rate of cycling is the same as it was in the second region while at the end of each charging period in the third region the battery gets fully charged.

Fig. 14 compares the SOC predictions obtained from the coulomb counting and extended Kalman filtering methods to the

Table 1
Summary of battery models.

Simple model:

$$SOC_{k+1} = SOC_k - \frac{\eta_i i_k \Delta t}{C_n}$$

$$V_k = OCV(SOC_k) - Ri_k$$

unable to follow the output voltage in constant voltage periods (not used).

Zero-state hysteresis model:

$$SOC_{k+1} = SOC_k - \frac{\eta_i i_k \Delta t}{C_n}$$

$$V_k = OCV(SOC_k) - Ri_k - s_k M$$

follow the output voltage in constant voltage periods, but, unable to follow the output voltage in dynamic environments (used).

Hysteresis model:

$$F(i_k) = \exp\left(-\left|\frac{\eta_i i_k \Delta t}{C_n}\right|\right)$$

$$\begin{bmatrix} h_{k+1} \\ SOC_{k+1} \end{bmatrix} = \begin{bmatrix} F(i_k) & 0 \\ 0 & 1 \end{bmatrix} \begin{bmatrix} h_k \\ SOC_k \end{bmatrix} + \begin{bmatrix} 0 & (1 - F(i_k)) \\ -\frac{\eta_i i_k \Delta t}{C_n} & 0 \end{bmatrix} \begin{bmatrix} i_k \\ M_k \end{bmatrix}$$

$$V_k = OCV(SOC_k) - Ri_k + h_k$$

follows the output voltage in both constant voltage periods and dynamic environments (used).

Table 2
Extended Kalman filtering for zero-state hysteresis model [26].

Nonlinear state-space model

$$SOC_{k+1} = SOC_k - \frac{\eta_i i_k \Delta t}{C_n} + w_k$$

$$V_k = OCV(SOC_k) - Ri_k - s_k M + v_k$$

where w_k and v_k are independent, zero-mean, Gaussian noises with covariance matrices P_v and P_w, respectively.

Definitions

$$\hat{C}_k = \frac{\partial OCV(SOC_k)}{\partial SOC_k}|_{SOC_k = \hat{SOC}_k^-}$$

Initialization ($k = 0$)

$$\hat{SOC}_0^+ = \mathbb{E}[SOC_0]$$

$$P_{\hat{SOC},0}^+ = \mathbb{E}[(SOC_0 - \hat{SOC}_0^+)(SOC_0 - \hat{SOC}_0^+)^T]$$

Computation ($k = 1,2,\ldots$)

Time updates

$$\hat{SOC}_k^- = \hat{SOC}_{k-1}^+ - \frac{\eta_i i_{k-1} \Delta t}{C_n}$$

$$P_{\hat{SOC},k}^- = P_{\hat{SOC},k-1}^+ + P_w$$

Measurement updates

$$L_k = P_{\hat{SOC},k}^- \hat{C}_k^T [\hat{C}_k P_{\hat{SOC},k}^- \hat{C}_k^T + P_v]^{-1}$$

$$\hat{SOC}_k^+ = \hat{SOC}_k^- + L_k[V_k - OCV(SOC_k) + Ri_k + s_k M]$$

$$P_{\hat{SOC},k}^+ = (1 - L_k \hat{C}_k) P_{\hat{SOC},k}^-$$

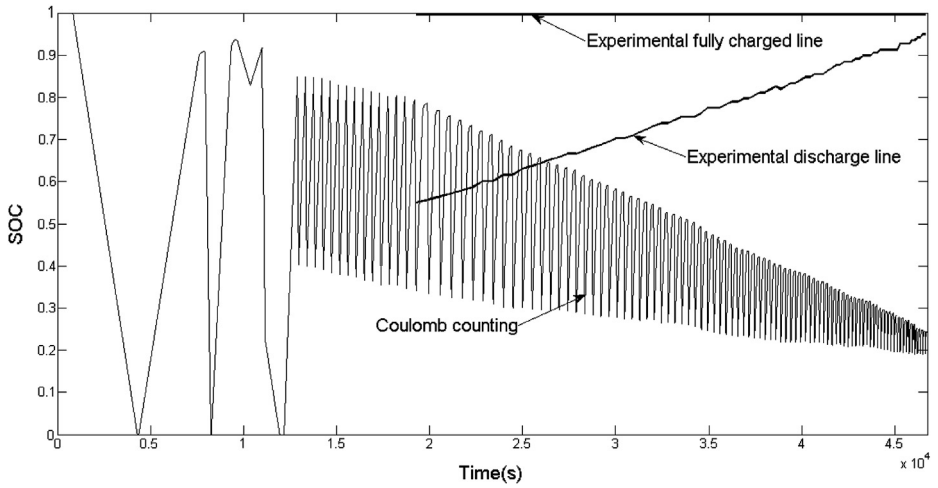

Fig. 12. SOC estimation using coulomb counting method.

experimental discharge line in the third region. Good agreement between the SOC estimation obtained from the extended Kalman filter method and the experimental discharge line (less than 1% error) is observed in this figure. Although the prediction obtained from the extended Kalman filtering is accurate in the third region, the results show inaccuracy in the second region. As discussed, the battery does not get fully charged in second region while the extended Kalman filter predictions reported in Fig. 13 show an opposite behavior. This deviation suggests poor voltage prediction of the zero-state model. Even with some weaknesses observed in the results of the proposed extended Kalman filter, it is superior to the common methods of the SOC estimation.

In order to apply the Kalman filtering method to the hysteresis-state model, the extended Kalman filter cannot be used since the parameters of the model are not constant. For the hysteresis-state model the Kalman filter has to identify the system parameters and also estimate the states of the system. Two main approaches have been taken by the researchers in dealing with this type of problems. First, the joint Kalman filtering which estimates both parameters and states of the system using a single Kalman filter. In this method, the parameters and states form a larger state vector which is estimated by a Kalman filter [28]. Second, the dual Kalman filtering whose algorithm is described in Fig. 15. In Fig. 15 the x represents the states of the system, θ is parameters of the system and P is the error covariance. In fact, this method starts with the time update of the parameters; then, the updated parameters are used to update the states in time. Finally, both states and parameters are updated employing the output measurement. Because the dual Kalman filtering uses the most updated estimate in each iteration, it is expected to achieve the better estimations; it is used in this study.

More importantly, the dual extended Kalman filtering is used due the existence of the system nonlinearity. The details of the filtering method are not described here, and more studies on dual extended Kalman filter can be find in [8,29,30]. The implementation of the dual extended Kalman filter using the hysteresis-state battery model is summarized in Table 3 where functions $f(.)$ can be obtained from Table 1. In this filter, it is assumed that the parameters of the battery change very slowly during the time and the driving process may be captured by just a small noise r_k. Therefore, the process model for the parameter identification has the form of $\theta_{k+1} = \theta_k + r_k$. In Table 3 the vector of the parameters, states and inputs are

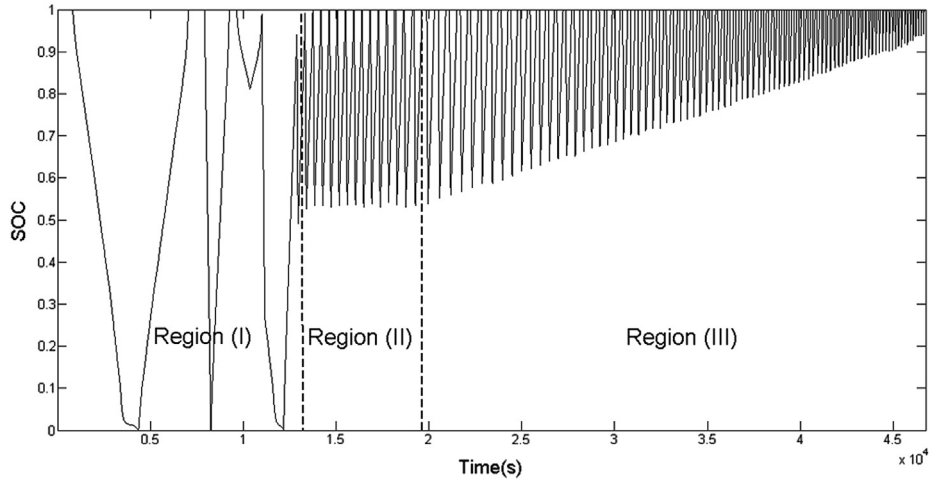

Fig. 13. SOC estimation using extended Kalman filter in three regions of experiment. Three regions include: (I) slow rate cycling region; (II) fast rate cycling region; and (III) fast rate cycling region with fully charging periods.

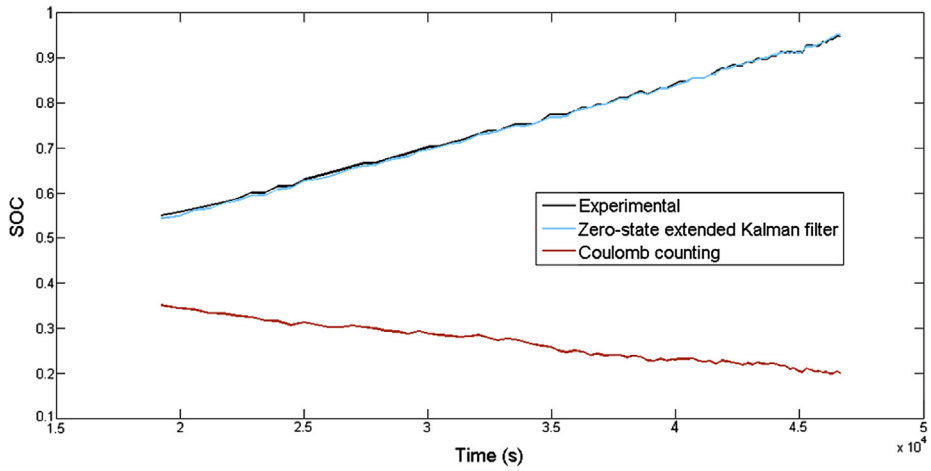

Fig. 14. Comparing the results obtained from the experimental data, coulomb counting method and extended Kalman filtering.

$$\theta_k = \begin{bmatrix} R_k^+ \\ R_k^- \\ M_k \\ \gamma_k \end{bmatrix}, x_k = \begin{bmatrix} h_k \\ \mathrm{SOC}_k \end{bmatrix}, u_k = \begin{bmatrix} i_k \\ M_k \end{bmatrix}$$

The matrix A_{k-1} is also as follows:

$$A_{k-1} = \begin{bmatrix} F(i_{k-1}) & 0 \\ 0 & 1 \end{bmatrix}$$

The dual extended Kalman filter mentioned in Table 3 estimates the states and parameters of the system in such a way that the model follows the measured input and outputs as close as possible. As a result, this filter may yield estimations which have no direct physical representation. To ensure the filter converges to the voltage estimation that has physical meaning Plett [8] suggested adding an additional equation to the measurement model within the Kalman filter method. This extra equation is a rough estimation of the battery terminal voltage.

$$V_k \approx \mathrm{OCV}(\mathrm{SOC}_k) - Ri_k$$
$$\mathrm{OCV}(\mathrm{SOC}_k) \approx V_k - Ri_k$$
$$\widehat{\mathrm{SOC}}_k - \mathrm{OCV}^{-1}(V_k + Ri_k)$$

By using the measures V_k, i_k and R from the previous step of dual extended Kalman filter, a rough estimation of the SOC is obtained which is enough to make the model converge to the true states. Consequently, adding this model to the hysteresis state model defines the function $g(.)$ used in Table 3.

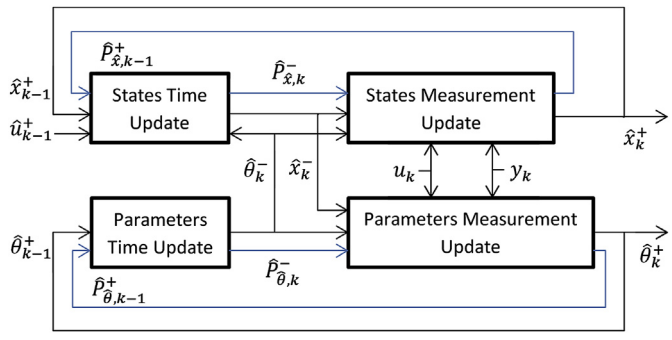

Fig. 15. Dual Kalman filter [8].

$$g(x_k, u_k, \theta) = \begin{bmatrix} \mathrm{OCV}(\mathrm{SOC}_k) - Ri_k + h_k \\ \mathrm{SOC}_k \end{bmatrix}$$

The measured output vector is also modified as

$$y_k = \begin{bmatrix} V_k \\ \widehat{\mathrm{SOC}}_k \end{bmatrix}$$

Then, the known function $g(.)$ is differentiated to obtain the C_k^x and C_k^θ.

Table 3
Dual extended Kalman filtering [29].

Nonlinear state-space models

$x_{k+1} = f(x_k, u_k, \theta_k) + w_k, \theta_{k+1} = \theta_k + r_k$

$y_k = g(x_k, u_k, \theta_k) + v_k, d_k = g(x_k, u_k, \theta_k) + e_k$

where w_k, v_k, r_k, and e_k are independent, zero-mean, Gaussian noises with covariance matrices P_v, P_w, P_r, and P_e, respectively

Definitions

$$A_{k-1} = \frac{\partial f(x_{k-1}, u_{k-1}, \widehat{\theta}_k^-)}{\partial x_{k-1}}\Big|_{x_{k-1}=\widehat{x}_{k-1}^+}$$

$$\widehat{C}_k^x = \frac{\partial g(x_k, u_k, \widehat{\theta}_k^-)}{\partial x_k}\Big|_{x_k=\widehat{x}_k^-}$$

$$\widehat{C}_k^\theta = \frac{\mathrm{d}g(x_k, u_k, \theta)}{\partial \theta}\Big|_{\theta_k=\widehat{\theta}_k^-}$$

Initialization ($k=0$)

$$\widehat{\theta}_0^+ = \mathbb{E}[\theta_0], P_{\widehat{\theta},0}^+ = \mathbb{E}[(\theta_0 - \widehat{\theta}_0^+)(\theta_0 - \widehat{\theta}_0^+)^T]$$

$$\widehat{x}_0^+ = \mathbb{E}[x_0], P_{\widehat{x},0}^+ = \mathbb{E}[(x_0 - \widehat{x}_0^+)(x_0 - \widehat{x}_0^+)^T]$$

Computation ($k=1,2,\ldots$)

Time updates for parameters

$$\widehat{\theta}_k^- = \widehat{\theta}_{k-1}^-$$
$$P_{\widehat{\theta},k}^- = P_{\widehat{\theta},k-1}^+ + P_r$$

Time updates for states

$$\widehat{x}_k^- = f(\widehat{x}_{k-1}^+, u_{k-1}, \widehat{\theta}_k^-)$$
$$P_{\widehat{x},k}^- = A_{k-1} P_{\widehat{\theta},k-1}^+ A_{k-1}^T + P_w$$

Measurement updates for states

$$L_k^x = P_{\widehat{x},k}^- (C_k^x)^T [C_k^x P_{\widehat{x},k}^- (C_k^x)^T + P_v]^{-1}$$
$$\widehat{x}_k^+ = \widehat{x}_k^- + L_k^x [y_k - g(\widehat{x}_k^-, u_k, \widehat{\theta}_k^-)]$$
$$P_{\widehat{x},k}^+ = (I - L_k^x C_k^x) P_{\widehat{x},k}^-$$

Measurement updates for parameters

$$L_k^\theta = P_{\widehat{\theta},k}^- (C_k^\theta)^T [C_k^\theta P_{\widehat{x},k}^- (C_k^\theta)^T + P_v]^{-1}$$
$$\widehat{\theta}_k^+ = \widehat{\theta}_k^- + L_k^\theta [y_k - g(\widehat{x}_k^-, u_k, \widehat{\theta}_k^-)]$$
$$P_{\widehat{\theta},k}^+ = (I - L_k^\theta C_k^\theta) P_{\widehat{\theta},k}^-$$

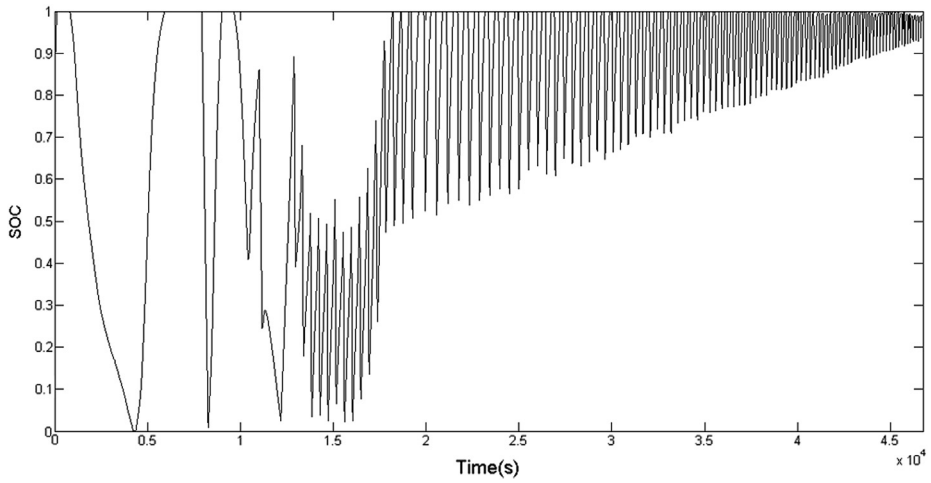

Fig. 16. SOC estimation using dual extended Kalman filter.

$$C_k^x = \begin{bmatrix} 1 & \dfrac{\partial \mathrm{OCV(SOC)}}{\partial \mathrm{SOC}} \\ 0 & 1 \end{bmatrix}_{\mathrm{SOC}=\widehat{\mathrm{SOC}}_k^-}$$

where ∂OCV(SOC)/∂SOC is calculated using the right hand side of the Eq. (8) Finally, the C_k^θ in Table 3 is calculated by utilizing the chain rule as follows:

$$C_k^\theta = \frac{\mathrm{d}g(\hat{x}_k^-, u_k, \theta)}{\mathrm{d}\theta}\Big|_{\theta=\hat{\theta}_k^-}$$

$$\frac{\mathrm{d}g(\hat{x}_k^-, u_k, \theta)}{\mathrm{d}\theta} = \frac{\partial g(\hat{x}_k^-, u_k, \theta)}{\partial \theta} + \frac{\partial g(\hat{x}_k^-, u_k, \theta)}{\partial \hat{x}_k^-}\frac{\mathrm{d}\hat{x}_k^-}{\mathrm{d}\theta}$$

$$\frac{\mathrm{d}\hat{x}_{k-1}^+}{\mathrm{d}\theta} = \frac{\mathrm{d}\hat{x}_{k-1}^-}{\mathrm{d}\theta} - L_{k-1}^x C_{k-1}^\theta$$

$$\frac{d\hat{x}_k^-}{d\theta} = \frac{\partial f\left(\hat{x}_{k-1}^+, u_{k-1}, \theta\right)}{\partial \theta} + \frac{\partial f\left(\hat{x}_{k-1}^+, u_{k-1}, \theta\right)}{\partial \hat{x}_{k-1}^+}\frac{\mathrm{d}\hat{x}_{k-1}^+}{\mathrm{d}\theta}$$

Here, it is assumed that the L_{k-1}^x is not function of θ and adding more derivatives will not improve the accuracy of the filter. For the hysteresis-state model, the above differentiations are obtained as

$$\frac{\partial g\left(\widehat{x}_k^-, u_k, \theta\right)}{\partial \theta} = \begin{bmatrix} -i_k^+ & -i_k^- & 0 & 0 \\ 0 & 0 & 0 & 0 \end{bmatrix}$$

$$\frac{\partial g\left(\widehat{x}_k^-, u_k, \theta\right)}{\partial \widehat{x}_k^-} = \begin{bmatrix} 1 & \dfrac{\partial \mathrm{OCV(SOC)}}{\partial \mathrm{SOC}} \\ 0 & 0 \end{bmatrix}_{\mathrm{SOC}=\widehat{\mathrm{SOC}}_k^-}$$

$$\frac{\partial f\left(\widehat{x}_{k-1}^+, u_{k-1}, \theta\right)}{\partial \theta} = \begin{bmatrix} 0 & 0 & (1-F_{k-1})\mathrm{sgn}(i_{k-1}) & \left(M - \widehat{h}_{k-1}^+\right)\left|\dfrac{\eta_i i_{k-1}\Delta t}{C_n}\right|F_{k-1} \\ 0 & 0 & 0 & 0 \end{bmatrix}$$

$$\frac{\partial f\left(\widehat{x}_{k-1}^+, u_{k-1}, \theta\right)}{\partial \widehat{x}_{k-1}^+} = \begin{bmatrix} F_{k-1} & 0 \\ 0 & 1 \end{bmatrix}$$

Now, the dual extended Kalman filter is implemented to estimate the SOC of the battery. Fig. 16 shows the result of applying the dual extended Kalman filter to the SOC estimation. The variation of the SOC depicted in Fig. 16 for the period of 12,000 s to 19,000 s, second region, does not show the problem reported in Fig. 13 for the same period of time. On the other hand, the close examination of the measured voltage, measured current, and the OCV curve of the battery suggests that the dual extended Kalman filtering method correctly captures the actual SOC of the battery in this period. Fig. 17 compares the experimental discharge line and the results obtained from the dual extended Kalman filter method. Good agreement between the discharge line and estimated SOC (less than 4%) is observed. Therefore, the dual extended Kalman filtering process is able to accurately track the behavior of the battery and can consequently be employed as a reliable SOC estimator in the dynamic environment of a HEV or PHEV.

5. Application of the model to A123 prismatic cells

In the next step, the proposed method is employed for the A123 prismatic batteries during different charge and discharge cycles. This is performed in order to clarify the performance of the developed dual extended Kalman filter in observing the SOC of different types of batteries. These batteries contain similar cathode chemistry of $LiFePO_4$ and their nominal voltage and capacity are 4.2 V and 20 Ah, respectively. The experimental data contain a US06 drive cycle, which is typically used to test vehicles at high speed and aggressive driving conditions. Figs. 18–20 show experimental measurements for current and voltage together with the simulation results for this drive cycle. The filter shows a good

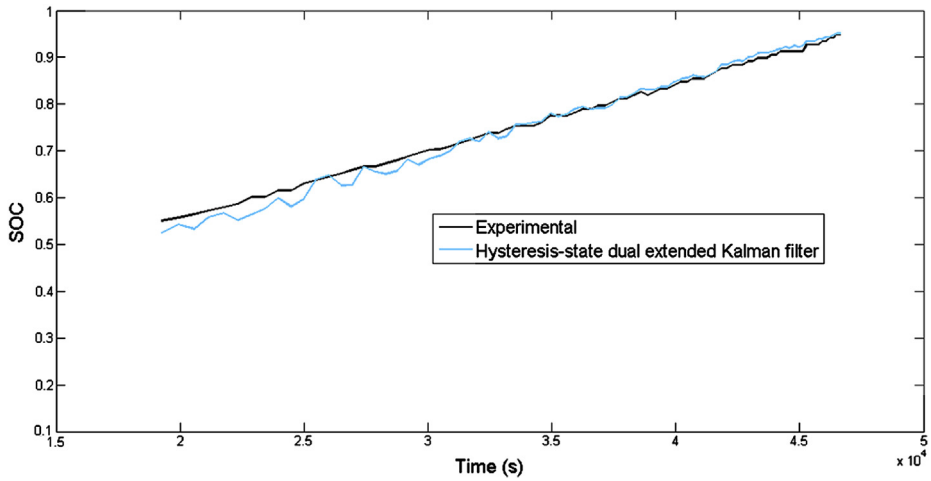

Fig. 17. Comparing the results obtained from the experimental data and dual extended Kalman filtering.

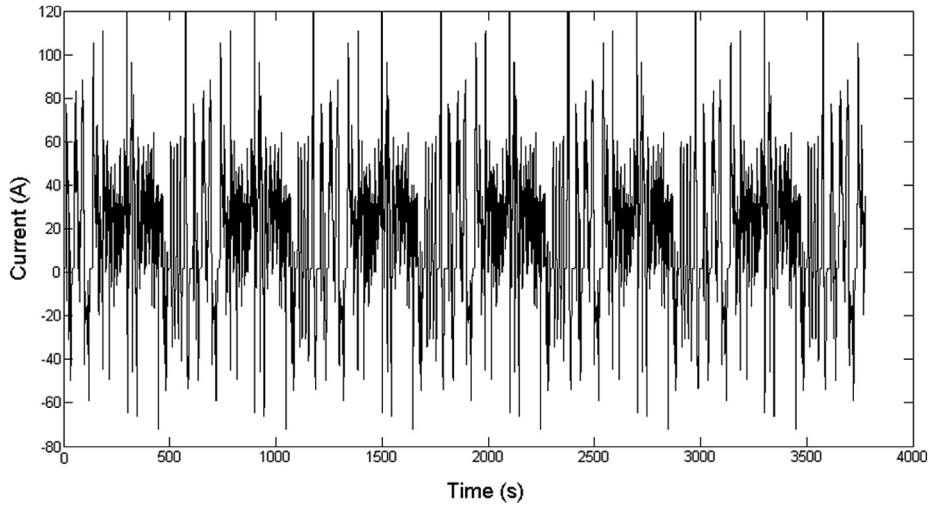

Fig. 18. Measured current profile for the prismatic Li-ion batteries with $LiFePO_4$ cathode over the US-06 drive cycle.

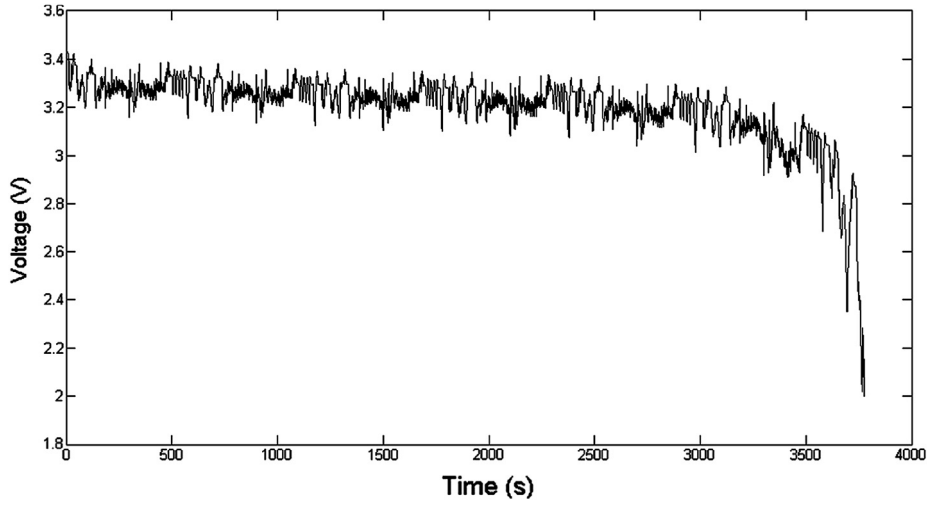

Fig. 19. Measured voltage profile for the prismatic Li-ion batteries with $LiFePO_4$ cathode over the US-06 drive cycle.

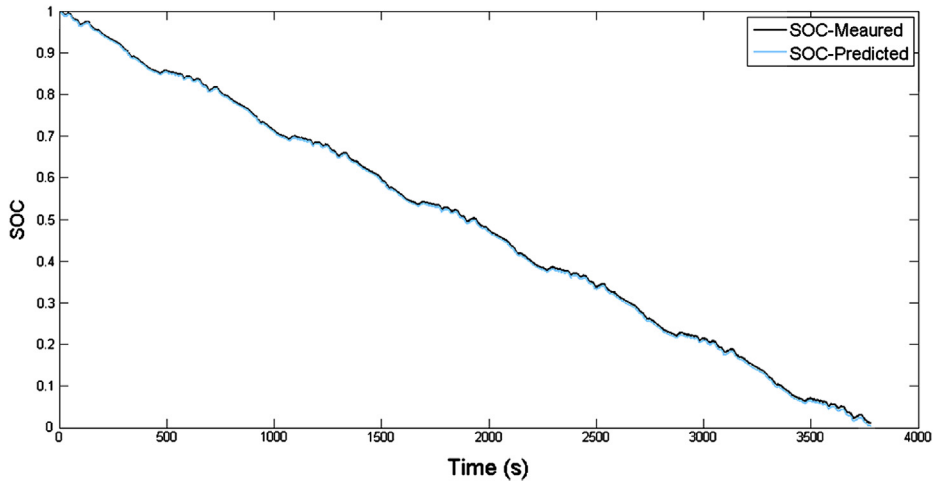

Fig. 20. SOC prediction using the dual extended Kalman filtering for the prismatic Li-ion batteries with $LiFePO_4$ cathode over US-06 drive cycle.

performance through cycling and can successfully simulates the measured SOC obtained by coulomb counting method using an accurate current sensor. These results show the effectiveness of applying the developed method on both types of $LiFePO_4$ batteries. In fact, the designed observers are only different in some parameters. These parameters are OCV of the battery as function of SOC, capacity of the cell, and must-be-tuned covariance matrices. The first two parameters are properties of the battery while the covariance matrices are utilized as the part of the process and measurement model explained in Table 3. These matrices are diagonal whose elements are presented in Table 4, P^i represents the ith element on the diagonal of the matrix. It should be noted that the covariance of the current and voltage vector measurements, P_w^2, P_v^1 and P_e^1, are set to the same values as in the previous test.

Moreover, the parameters P_r^1 and P_r^2 shown in Table 4 are the driving terms to update the internal resistances as a function of time. When these values decrease to 1.3×10^{-15} for the cylindrical cells, similar results are obtained in the extended Kalman filter with fixed-parameters. Table 4 shows that these two parameters can be up to three orders of magnitude larger for cylindrical cells than prismatic. These differences clearly suggest different magnitudes for the internal resistances operating within each battery during cycling.

Since both batteries (cylindrical and prismatic batteries of A123™) contain $LiFePO_4$ cathodes, the variation of these parameters is the result of distinct properties varying with geometry and electrode thickness, and whose impacts affect significantly the impedance of the batteries. It is known that cylindrical cells present a higher volume to outer surface ratio compared to the prismatic cells. Consequently, the heat generated during the operation of the cylindrical batteries would not be transferred to the outside as fast as in prismatic cells, and thus the temperature of cylindrical batteries increases more than the prismatic ones during the cycling process. The temperature rise in these batteries both depends on, and influences their internal resistance, and this property can be utilized as an indicator of the impedance presents within each battery. Note that the cathode material for both batteries is the $LiFePO_4$ phase ($0.005\ S\ m^{-1}$) which is generally a poor electronic conductor. Thus, several methods are needed to be implemented in order to increase its conductivity (e.g. carbon mixing, doping, particle size reduction) [31,32]. Undoubtedly, the application of these treatments at different scales or geometries (e.g. between cylindrical and prismatic batteries) modifies significantly the conductivity and other phenomena (e.g. diffusion, volume expansion of the cathode material) inside the batteries, and accordingly the extent of the impedance. Experimental evidence combined with model simulations has revealed that this type of transport limitations of the cathode material can also restrict the power of the batteries [33]. A similar situation might arise from variations in the electrolyte conductivity among the batteries. Therefore, it is not surprising to observe a variation between the parameters describing the behavior of these batteries, as a result of their reliance upon geometry-dependent impedances (and other factors affecting them).

The analysis of the filter parameters constitutes the first step to apply the method developed in this work for SOC estimation. This can be achieved via some trial-and-error initial studies. Once these parameters are established for the specific cell geometry and materials, the filter can be used to predict the SOC of the battery at different working situations. In addition, since the Li-ion batteries present in general the same controlling phenomena with different magnitudes due to modifications of the electrode materials, most likely, the method presented in this study could also be used for other type of batteries containing different cathode materials (e.g. Li_2MnO_4, $LiCoO_2$, NMC).

Table 4
Parameters of the dual extended Kalman filters for cylindrical and prismatic Li-ion batteries

Parameters	Cylindrical battery	Prismatic battery
P_w^1	1.3×10^{-4}	1.3×10^{-8}
P_r^1	1.3×10^{-10}	1.3×10^{-13}
P_r^2	1.3×10^{-10}	1.3×10^{-13}
P_r^3	1.3×10^{-6}	1.3×10^{-8}
P_r^4	1.3×10^{-6}	1.3×10^{-8}
P_v^2	1.8×10^{-4}	1.8×10^{-4}
P_e^2	1.8×10^{-4}	1.8×10^{-4}

6. Conclusion

In this paper, a method based on the Kalman filtering theory was developed to estimate SOC in a battery management system (BMS) for $LiFePO_4$ cells, and this method was applied to both cylindrical and prismatic cells. Three models were utilized and compared each other to describe the battery dynamics in a hybrid electric (HEV) or plug-in hybrid electric vehicle (PHEV). It was found that the simple model presents a deviation in the constant voltage charging periods, whereas the hysteresis-state model generates the best

predictions in both dynamic and static environments. The zero-state hysteresis and hysteresis-state models were subsequently implemented in two types of Kalman filtering processes in order to estimate the SOC of the battery. The extended Kalman filter was used in the case of the fixed-parameter (zero-state hysteresis) model, and the dual extended Kalman filter was employed for the varying-parameter (hysteresis-state) model. In the dual method, the model parameters and the SOC of the battery were simultaneously estimated using Kalman filtering. The implementation of both filters was described in detail and then the results of the Kalman filtering were compared with experimental data. Good agreement (less than 4%) was observed between Kalman filtering methods and the experimental data, indicates that the proposed methods can properly predict the SOC of the battery under dynamic environments such as in a PHEV application. Accordingly, it can be effectively used in BMS. The method was also employed to predict the SOC of a prismatic cell, showing the filter capabilities to estimate the SOC for different types of batteries. Analysis of the parameters calculated by the filter revealed that these values depend on the type of battery (e.g. geometrical factors varying their properties). However, these parameters can be quickly determined from an initial study of a specific cell configuration, and subsequently used for that cell type under other operating conditions.

References

[1] J. Zhang, J. Lee, J. Power Sources 196 (2011) 6007–6014.
[2] Y. Barsukov, Texas Instrument Workbook (2004) Chapter (1-1)–(1-9).
[3] G. Plett, J. Power Sources 134 (2004) 252–261.
[4] S. Pang, J. Farrell, J. Due, M. Barth, Proceeding of the American Control Conference, Arlington, VA, 2001, pp. 25–27.
[5] K. A. Smith, C. D. Rahn, C. Y. Wang, IEEE International Conference on Control Application, 2008, pp. 714–719.
[6] D.D. Domenico, A. Stefanopoulou, G. Fiengo, J. Dyn. Syst. Meas. Control 132 (6) (2010) 061302.
[7] S. Lee, J. Kim, J. Lee, B. Cho, J. Power Sources 185 (2008) 1367–1373.
[8] G. Plett, J. Power Sources 134 (2004) 277–292.
[9] G. Plett, J. Power Sources 161 (2006) 1356–1368.
[10] G. Plett, J. Power Sources 161 (2006) 1369–1384.
[11] D. Andre, C. Appel, T. Soczka-Guth, D.U. Sauer, J. Power Sources 224 (2013) 20–27.
[12] W. He, N. Williard, C. Chen, M. Pecht, Microelectronic Reliability (2013). Available online at: http://dx.doi.org/10.1016/j.microrel.2012.11.010.
[13] S. Yuan, H. Wu, C. Yin, Energies 6 (2013) 444–470.
[14] S. Piller, M. Perrin, A. Jossen, J. Power Sources 96 (2001) 113–120.
[15] M. Stevens, Ph.D. thesis, University of Waterloo (2008).
[16] S. Rodrigues, N. Munichandraiah, A. Shukla, J. Power Sources 87 (2000) 12–20.
[17] F. Huet, J. Power Sources 70 (1998) 59–69.
[18] S. Rodrigues, N. Munichandraiah, A. Shukla, J. Solid State Electrochem 3 (1999) 397–405.
[19] A. Zenati, Ph. Desprez, H. Razik, S. Rael, IEEE vehicle Power and Propulsion Conference (2010), Article number: 5729069.
[20] B. Saha, K. Goebel, "Battery Data Set", NASA Ames Prognostics Data Repository, NASA Ames, Moffett Field, CA, 2007. http://ti.arc.nasa.gov/project/prognostic-data-repository.
[21] N. Watrin, B. Blunier, A. Miraoui, Transportation Electrification Conference and Expo (ITEC), 2012 IEEE, pp.1–6, 18–20 June 2012.
[22] M.Wahlstrom, Master's thesis, University of Waterloo (2010).
[23] http://www.a123systems.com/.
[24] S. Santhanagopalan, R.E. White, J. Power Sources 161 (2006) 1346–1355.
[25] S.K. Rahimian, S. Rayman, R.E. White, J. Electrcochem. Soc. 159 (2012) A860–A872.
[26] G. Plett, J. Power Sources 134 (2004) 262–276.
[27] D. Simon, Optimal State Estimation: Kalman, H-infinity, and Nonlinear Approaches, John Wiley & Sons, 2006.
[28] G. L. Plett, Patent No.: US 7,593,821 B2 (2009).
[29] E.A. Wan, A.T. Nelson, Kalman Filtering and Neural Networks, John Wiley & Sons, 2001, pp. 123–173. (Chapter 5).
[30] A. Nelson, Ph.D. thesis, Oregon Graduate Institute of Science and Technology (2000).
[31] W.B. Gu, C.Y. Wang, in: Lithum Batteries, The Electrochemical Society Proceedings Series, vol. PV 99-25, The Electrochemical Society, Pennington, NJ, 1999, p. 748.
[32] W.A. van Schalkwijk, B. Scrosati (Eds.), Kluwer Academic Publishers, New York, 2002.
[33] V. Srinivasan, J. Newman, J. Electrochem. Soc. 151 (2004) A1530–1538.

Nomenclature

δ: arbitrary small number
Δt: time step
η_i: coulombic efficiency of the battery
γ: tuning factor in hysteresis state model
$\mathbb{E}$: expectation operator
θ_k: vector of parameters in kth time step
C_n: nominal capacity of the battery
d_k: vector of outputs in kth time step
e_k: independent, zero-mean, Gaussian noise in the measurement model of Kalman filter
$f(.)$: process model function for the states
$g(.)$: measurement model function
h: hysteresis state
I: current of the battery and identity matrix
i_k: current of the battery in kth time step
L_k: Kalman gain matrix in kth time step
M: hysteresis
P_e: covariance matrix of process noise
P_r: covariance matrix of measurement noise
P_v: covariance matrix of measurement noise
P_w: covariance matrix of process noise
R^+: internal resistance of the battery during discharging
R^-: internal resistance of the battery during charging
r_k: independent, zero-mean, Gaussian noise in the process model of Kalman filter
sgn: sign function
t: time
u_k: vector of inputs in kth time step
V_k: terminal voltage of the battery in kth time step
v_k: independent, zero-mean, Gaussian noise in the measurement model of Kalman filter
w_k: independent, zero-mean, Gaussian noise in the process model of Kalman filter
x_k: vector of states in kth time step
y_k: vector of outputs in kth time step